



A Journal of the Gesellschaft Deutscher Chemiker

Angewandte Chemie

GDCh

International Edition

www.angewandte.org

Accepted Article

Title: Size-dependent activity and selectivity of atomic-level Cu nanoclusters during CO/CO₂ electroreduction

Authors: Weifeng Rong, Haiyuan Zou, Wenjie Zang, Shibo Xi, Shuting Wei, Baihua Long, Junhui Hu, Yongfei Ji, and Lele Duan

This manuscript has been accepted after peer review and appears as an Accepted Article online prior to editing, proofing, and formal publication of the final Version of Record (VoR). This work is currently citable by using the Digital Object Identifier (DOI) given below. The VoR will be published online in Early View as soon as possible and may be different to this Accepted Article as a result of editing. Readers should obtain the VoR from the journal website shown below when it is published to ensure accuracy of information. The authors are responsible for the content of this Accepted Article.

To be cited as: *Angew. Chem. Int. Ed.* 10.1002/anie.202011836

Link to VoR: <https://doi.org/10.1002/anie.202011836>

Size-dependent activity and selectivity of atomic-level Cu nanoclusters during CO/CO₂ electroreduction

Weifeng Rong,^{[a,b]†} Haiyuan Zou,^{[a,c]†} Wenjie Zang,^[d] Shibo Xi,^[e] Shuting Wei,^[a] Baihua Long,^[a] Junhui Hu,^[a] Yongfei Ji^[f] and Lele Duan^{*[a]}

[a] Dr. W. Rong, H. Zou, Dr. S. Wei, Dr. B. Long, J. Hu, Prof. Dr. L. Duan
Department of Chemistry and Shenzhen Grubbs Institute
Southern University of Science and Technology (SUSTech)
Shenzhen, Guangdong 518055, P. R. China
E-mail: duanll@sustech.edu.cn

[b] Dr. W. Rong
School of Chemistry and Materials Science
University of Science and Technology of China
Hefei, Anhui 230026, P. R. China

[c] H. Zou
School of Chemistry and Chemical Engineering
Harbin Institute of Technology
Harbin, Heilongjiang 150001, P. R. China

[d] W. Zang,
Department of Materials Science and Engineering, Faculty of Engineering
National University of Singapore
117574, Singapore

[e] S. Xi
Institute of Chemical and Engineering Sciences, Agency for Science
Technology and Research (A*STAR)
1 Pesek Road, Jurong Island 627833, Singapore

[f] Prof. Dr. Y. Ji
School of Chemistry and Chemical Engineering
Guangzhou University
Guangzhou, Guangdong 510006, P. R. China

†These authors contributed equally to this work.

Supporting information for this article is given via a link at the end of the document.

Abstract: As a favourite descriptor, the size effect of Cu-based catalysts has been regularly utilized for activity and selectivity regulation toward CO₂/CO electroreduction reactions (CO₂/CORR). However, little progress has been made in regulating the size of Cu nanoclusters at the atomic level. Here, the size-gradient Cu catalysts from single atoms (SAs) to subnanometric clusters (SCs, 0.5–1 nm) to nanoclusters (NCs, 1–1.5 nm) on graphdiyne matrix are readily prepared via a creative acetylenic-bond-directed site-trapping approach. Electrocatalytic measurements show a significant size effect in both the activity and selectivity toward CO₂/CORR. Increasing the size of Cu nanoclusters will improve catalytic activity and selectivity toward C₂₊ productions in CORR. A high C₂₊ conversion rate of 312 mA cm⁻² with the Faradaic efficiency of 91.2% are achieved at -1.0 V vs. reversible hydrogen electrode (RHE) over Cu NCs. The presented activity/selectivity-size relations provide a clear understanding of mechanisms in the CO₂/CORR at the atomic level.

Introduction

CO₂/CORR has triggered significant attention to realize the decarbonization roadmap using excess renewable electricity. To date, Cu-based catalysts have shown great promise for electrochemical reduction of CO₂/CO to synthesize high-value multicarbon (C₂₊) products owing to the moderate binding strength of intermediate evolutions, although oftentimes suffering from the low activity and selectivity.^[1] Nanostructuring of bulky Cu has also been widely applied in attempts to improve

the selectivity and geometric activity.^[2] The size effects on the reactivity of electrocatalysts have been extensively investigated. For example, Reske et al. demonstrated that a dramatic increase in the catalytic activity and selectivity for H₂ and CO was observed with decreasing Cu particle size in the 2–15 nm mean size range for CO₂RR.^[3] A recent study of CO₂RR indicated that small copper nanoparticles (25 nm) led to a high ethylene production with a remarkable high FE (92.8%).^[4] Emphasis on size-controlled Cu particles comes down to several reasons: (1) decreasing the size leads to the enhanced surface-to-volume ratio and thus improves the metal atoms utilization; (2) as the size of a particle decreases, the increasing undercoordinated sites lead to perturbed electronic structure and oftentimes increased reactivity;^[5] (3) varying size can influence the binding strength of the different reaction intermediates, and thus affect the final product selectivity.^[6]

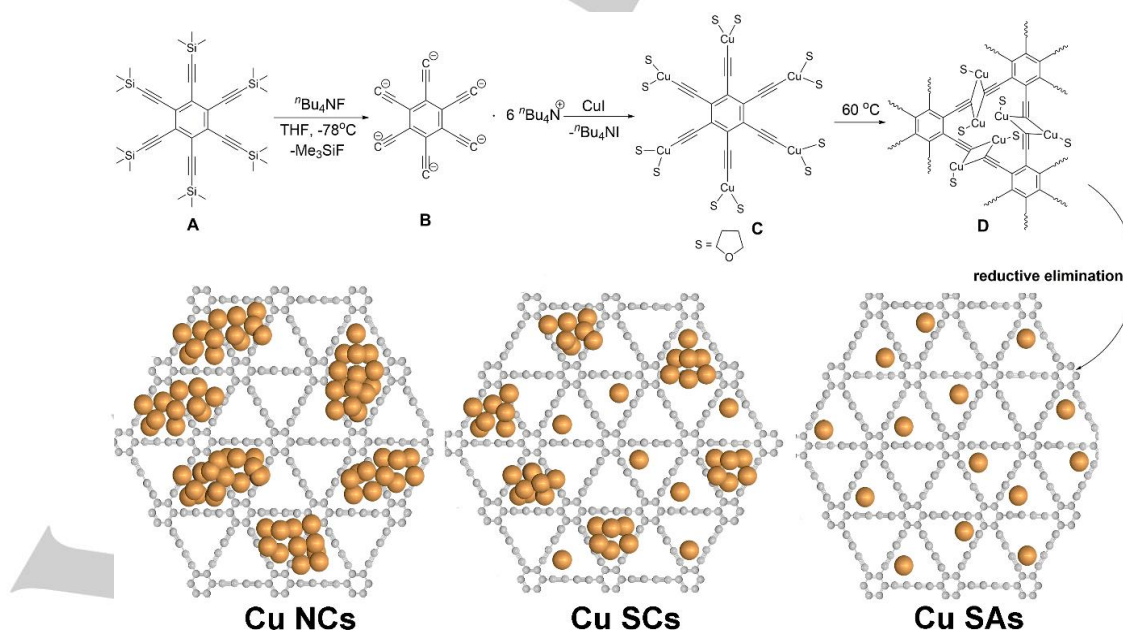
Inspired by these potential advantages, we attempt to explore the size effect of Cu nanoclusters (Cu NCs) in CO₂/CORR aiming at improving the electrocatalytic activity and boosting the C–C coupling reactions to form C₂₊ products. Compared to Cu NPs, the size effects of Cu NCs are less often examined due to the difficulty of their preparation. Yet the study on Cu NCs can provide a clear picture of well-defined local coordination environments of active sites, in favor of discovering the catalytic mechanism of CO₂ activation or CO dimerization at an atomic level.^[7] Recently, a series of structural models of Cu NCs have been evaluated by computational calculations to shed light on the size effect for the CO₂RR.^[8] Nevertheless, the experimental investigations are still lacking,^[9] and the relevant mechanisms remain elusive, leaving the size effect unexplored.

To prevent the Cu NCs from agglomeration into NPs, a suitable supporting material is required to efficiently stabilize small Cu NCs through strong metal-support interactions and meanwhile to maximum the undercoordinated active sites. Moreover, the supporting materials greatly contribute to the catalytic activity of the metal catalysts when particle size is smaller than 6 nm.^[10] Graphdiyne (GDY), first prepared by the Li group in 2010,^[11] can provide anchoring sites for immobilizing the metal atoms due to its rich triple bonds with strong electron-donating ability.^[12] In particular its uniformly distributed 18 C hexagonal pores not only confine active sites locally^[13] but also make the electrocatalytic performance in high durability under reaction conditions.^[14] These combined properties enable GDY to be a proper support to control the size of Cu active sites. However, to the best of our knowledge, no GDY-supported Cu NCs have been documented due to the lack of impactful synthetic strategies to prevent agglomeration of NCs to NPs under high loading.

In this study, a family of size-controlled Cu catalysts from single atoms (SAs) to subnanometric clusters (SCs, 0.5–1 nm) to nanoclusters (NCs, 1–1.5 nm) confined on GDY were synthesized via a general acetylenic-bond-directed site-trapping approach. In CO₂/CORR experiments, the product distribution strongly depends on the size of NCs. Typically, the catalyst with smaller NCs is less active and less selective for CO in favor of H₂ toward CO₂RR. For CORR, the increasing size allows for tuning of the C₂₊/C₁ ratio from 0.35 to 398.5 at –1.0 V vs. RHE and a decrease in CH₄ FE from 51.3% to 0.2%. Under the optimized conditions, we achieved an C₂₊ partial current density of 312 mA cm⁻² (1.0 M KOH, –1.0 V vs. RHE) and a FE of 93.9% (1.0 M KOH, –0.8 V vs. RHE) over Cu NCs. Moreover, the long-term stability of Cu NCs during electrolysis, realized by the strong coordination and confinement from GDY support, is also highlighted here. Cu catalysts presented here provide a unique opportunity to understand the mechanism of CO₂/CORR and their study is the first exploration of size effects of atomic-level Cu NCs.

Results and Discussion

Diverse preparation techniques for Cu NCs and SAs have emerged.^[15] These methods usually involve multistep procedures. More importantly, they cannot effectively prevent aggregation of the low coordinated Cu atoms during high-temperature calcination at increasing atom concentration. We introduce herein an acetylenic-bond-directed site-trapping method to synthesize GDY-supported Cu NCs and SAs in-situ. The formation of macromolecular GDY support and the anchoring of metal atoms concurred to ensure their compatibility throughout the reaction process (Scheme 1). Hexakis[(trimethylsilyl)ethynyl]benzene (**A**) is deprotected by ⁿBu₄NF; the resulting anionic intermediate **B** reacts with cuprous iodide (CuI) to afford the corresponding unstable copper (I)-σ-alkynyl complex **C**, which subsequently undergoes redox reaction via a π-alkyne binuclear species **D** to simultaneously generate Cu⁰ and GDY at elevated temperatures. These Cu⁰ atoms are prone to be trapped kinetically and tethered within the pores formed by three butadiyne linkages (–C≡C–C≡C–) between the benzene rings of GDY ascribing for the nanoconfinement effect and strong metal-support interactions. However, Cu atoms tend to gather into the corresponding bulk phase thermodynamically.^[16] Consequently, the balance of combined actions leads to the formation of Cu NCs or/and SAs under the varied amount of cuprous precursor (Figure S1, Supporting Information). We prepared three GDY-supported Cu catalysts (two different sized NC catalysts, one SA catalyst as a reference). Inductively coupled plasma atomic emission spectrometry measurement showed the Cu doping concentration of 45.2 wt %, 6.0 wt % and 1.5 wt % respectively on GDY, denoted as Cu_{45.2}/GDY (NCs), Cu_{6.0}/GDY (SCs) and Cu_{1.5}/GDY (SAs). It is noteworthy that Cu_{45.2}/GDY is the highest loading nanocluster catalyst reported thus far.



Scheme 1. Schematic illustration for the synthesis of Cu/GDY.

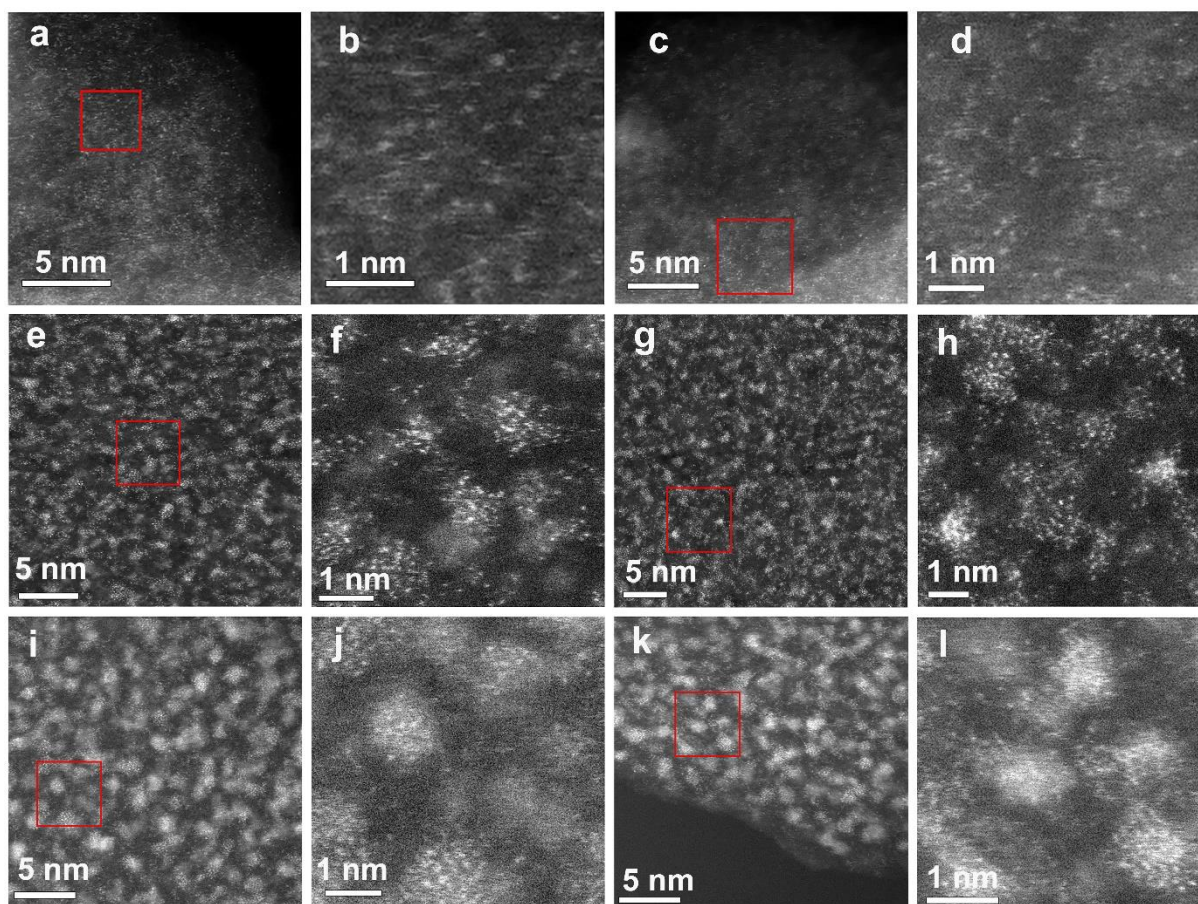


Figure 1. a–d) HAADF-STEM images of $\text{Cu}_{1.5}/\text{GDY}$ (SAs). e–h) HAADF-STEM images of $\text{Cu}_{6.0}/\text{GDY}$ (SCs). i–l) HAADF-STEM images of $\text{Cu}_{45.2}/\text{GDY}$ (NCs). a, c, e, g, i, k) HAADF-STEM images at low magnification. b, d, f, h, j, l) Corresponding enlargement of the marked regions in a, c, e, g, i, k), respectively.

Atomic-resolution high-angle annular dark-field scanning transmission electron microscopy (HAADF-STEM) reveals that the size of bright spots increases with gradually increasing Cu loading ranging from a single atomic to a subnanometric to a nanometric level (Figure 1). As shown in Figures 1a–d, the numerous individual Cu atoms can be clearly observed for $\text{Cu}_{1.5}/\text{GDY}$. A mixture of Cu SCs (0.5–1 nm) and SAs are well dispersed on the GDY surface for $\text{Cu}_{6.0}/\text{GDY}$ (Figures 1e–h). Cu NCs (1–1.5 nm) are evidently well-distributed throughout GDY framework for the highest loading (Figures 1i–l). X-ray diffraction (XRD) patterns (Figure S2) of three as-prepared catalysts show a typically sole broad peak for each Cu/GDY,^[13d] reflecting the predominant carbon support.^[17] The nature of carbonaceous materials of Cu/GDY is further authenticated by Raman spectroscopy (Figure S3). The distinct G band (1576–1588 cm^{-1}) and D band (1386–1394 cm^{-1}) represent the aromatic and disordered carbon respectively.^[11] The slight hypsochromic shift for the G bands on Cu/GDY reveals the charge transfer from Cu to GDY.^[13d] The decreasing intensity ratio of D and G bands for Cu/GDY at increasing loading conditions indicates a gradually diminished amount of defects in Cu/GDY,^[18] which should be ascribed to the nearly perfect reaction of the copper precursor with arylene monomer. Furthermore, the obvious peaks at 2170.6 cm^{-1} and 1974.8 cm^{-1} for $\text{Cu}_{45.2}/\text{GDY}$ confirm the formation of conjugated diyne linkers ($-\text{C}\equiv\text{C}-\text{C}\equiv\text{C}-$). X-ray photoelectron

spectroscopy (XPS) in Figure 2a shows identical peaks at ca. 932.7 eV for Cu $2p_{3/2}$, which is situated between Cu^0 (932.4 eV) and Cu^{2+} (934.6 eV),^[19] suggesting the ionic $\text{Cu}^{\delta+}$ ($0 < \delta < 2$) nature of copper. The peak centered at 915.9 eV in Cu LMM Auger spectrum (Figure S5b) further demonstrates the richness of $\text{Cu}^{\delta+}$ in Cu/GDY. The C 1s orbital that can be deconvoluted into four subpeaks are assigned to the C–C (sp^2), C–C (sp), C–O, and C=O (Figure S4b–e), respectively. The area ratios of sp peak and sp^2 peak are close to 2, indicating the well-maintained GDY skeleton.

X-ray absorption spectroscopy (XAS) was further introduced to investigate the chemical nature and structure of Cu species at the atomic scale. Figure 2b shows the Cu k -edge XANES spectra of Cu foil, CuI and Cu/GDY. The near-edge features of Cu/GDY are in between of those of Cu foil and CuI, indicating that the Cu species are partially positively charged ($\text{Cu}^{\delta+}$, $0 < \delta < 1$) due to the charge redistribution between Cu^0 and GDY,^[13a] in agreement with XPS analysis. Fourier-transformed k^3 -weighted extended X-ray absorption fine structure (EXAFS) in R space showed only one notable peak at 1.47 Å from the first coordination shell of Cu–C bond for Cu/GDY (Figure 2c), very close to that of the nanodiamond-graphene supported Cu SACs (1.5 Å).^[19b] $\text{Cu}_{45.2}/\text{GDY}$ and $\text{Cu}_{6.0}/\text{GDY}$ respectively display an additional minor peak at 2.3 Å and 2.2 Å, ascribed to Cu–Cu scattering, confirming the formation of Cu_n clusters. By contrast,

no obvious peaks at 2.2–2.3 Å for Cu_{1.5}/GDY evidenced that Cu atoms are atomically dispersed, in accordance with the HAADF-STEM observations.

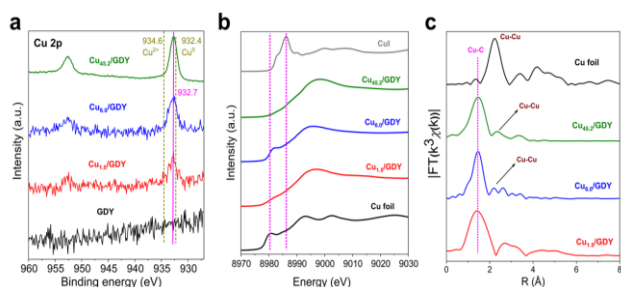


Figure 2. Structural characterizations of Catalysts. a) The narrow scan XPS spectra for Cu 2p of Cu/GDY. b) Cu *k*-edge X-ray absorption near-edge structure (XANES). c) FT *k*²-weighted extended X-ray absorption fine structure (EXAFS) spectra of Cu/GDY and the reference Cu foil.

The CO electrocatalytic performance of Cu/GDY and GDY was investigated using a three-compartment flow electrolyser (Figure S8). Initially, the electrocatalytic performances of Cu/GDY and GDY were examined in 0.1 M KOH solution. The results are summarized in Figure 3. Cu/GDY showed good catalytic activities for CORR and high total FE_s spanning a very wide potential window (Figure S9). The products detected in significant quantities are methane (CH₄), ethanol, acetate, ethylene (C₂H₄), *n*-propanol (*n*-PrOH) as well as H₂ (Figure S16, S20–S22). A drastic rise of the C₂₊ FE_s at the expense of methane is observed with the increasing size of Cu NCs. Cu SAs (Cu_{1.5}/GDY) shows a remarkable FE (57.3%) of C₁ (CH₄) as a major product at –1.0 V vs. RHE (Figure 3a) vs. the FE (20%) for C₂, with a C₂₊/C₁ ratio of 0.35 (Figure 3d) and no *n*-PrOH is observed. When the small SCs are emerging (Cu_{6.0}/GDY)

(Figure 3b), substantial loss of the CH₄ selectivity is observed along with the enhanced FE of C₂ compounds. The relative ratio of C₂₊/C₁ is hiked from 0.35 to 2.72 at the same potential. Similar trends can further be seen for NCs (Cu_{45.2}/GDY) (Figure 3c). Interestingly, CH₄ is almost completely eliminated except at more negative potentials^[2c]. In sharp contrast, C₂₊ compounds are constituting about 80% out of the total products generated, whilst hydrogen evolution is hovering around the lowest level at a wide potential window in comparison with the other two catalysts. C₂H₄ and *n*-PrOH productions are respectively increasing up to the maximum FE_s of 40.4% and 12.8% under appropriate potentials (Figure S14). Our results have demonstrated a clear size dependence of activity and selectivity toward CORR over Cu nanocluster catalysts below 2 nm for the first time.

As is known to all, highly alkaline electrolyte greatly lowers the overpotential of formation of C₂₊ product and boosts a high rate of electrolysis.^[20] The higher electrolyte concentration (1.0 M KOH) was also employed to avoid mass transport limitation as well as to examine the influence of pH over the Cu NCs (Cu_{45.2}/GDY) for CORR (Figure 3e and S23). Overall, the total FE_s at every potential are close to 100%, revealing that the electrolysis proceeds better than that in 0.1 M KOH. Both the C₂₊ partial current density and FE increase with increasing the KOH concentration. The hydrogen evolution reaction (HER) is further suppressed. The C₂₊ FE reaches up to 93.9% at –0.8 V vs. RHE and the highest conversion rate rises to 312 mA cm⁻² at –1.0 V vs. RHE. This represents the Cu nanoclusters with the highest catalytic activity and C₂₊ selectivity to date for CORR. The FE of acetate is significantly improved in higher alkaline electrolyte, which is attributed to the suppression of H₂ and *n*-PrOH, indicating a high pH environment could reduce the absorption of H⁺ and make it difficult for C–C coupling of C₂ intermediate for propanol production with CO.^[6]

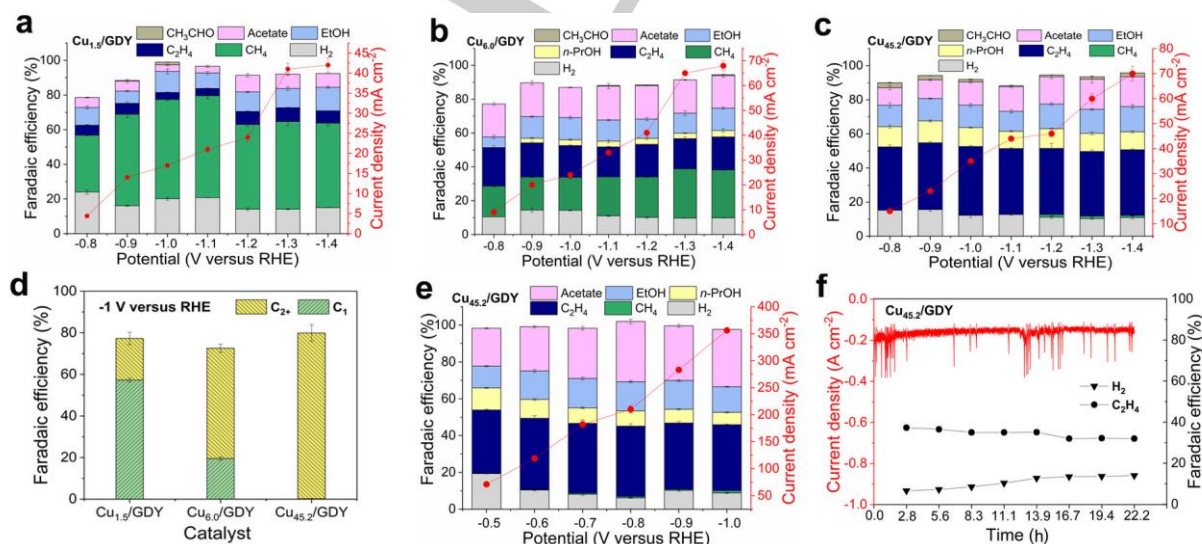


Figure 3. CO electroreduction performance of Cu/GDY. a–c) Total current density and cumulative FE_s vs. applied potential in 0.1 M KOH. d) C₂₊/C₁ ratios of different catalysts at –1.0 V vs. RHE. e) Total current density and cumulative FE_s vs. applied potential in 1.0 M KOH. f) Stability test of Cu_{45.2}/GDY with gas products measured every 10000 s in 1.0 M KOH at –0.8 V vs. RHE.

Long-term electrolysis was performed at a stationary -0.8 V vs. RHE for over 22 h to test the stability of $\text{Cu}_{45.2}/\text{GDY}$ in 1.0 M KOH electrolyte (Figure 3f). The total current densities fluctuate within $210\text{--}150$ mA cm^{-2} over the electrolysis course, which is caused by bubble accumulation in the liquid catholyte chamber.^[21] The slight changes in FEs of H_2 (6.6%–14%) and C_2H_4 (37.5%–32%) imply the decrease in C_{2+} selectivity due to flooding issues through the GDY into the CO gas chamber during the long-term high-rate electrolysis.^[2c, 21–22] XRD, XPS and HADDF-STEM characterization of $\text{Cu}_{45.2}/\text{GDY}$ samples after CORR were immediately carried out to examine if dynamic changes happened. The selfsame spectra (Figure S5, S6 and S7) reveal the robustness of Cu nanocluster catalysts during the CORR process in comparison with the as-prepared.

To better elucidate the nature and stability of as-prepared Cu/GDY with different sizes of NCs, we also examined catalytic performance for CO_2 reduction as a contrast in a CO_2 -saturated 0.5 M KHCO_3 (pH 7.2) during 1 h electrolysis (Figure S17). Different from CORR, only three electroreduction products in substantial quantities (H_2 , CO, formate) are detected at a wide potential window, C_2H_4 is found in a small quantity (FE < 3%) only if large overpotential is applied over $\text{Cu}_{45.2}/\text{GDY}$. The catalytic activity and selectivity are found to strongly vary as a function of the cluster size. As shown in Figure S17a, all three Cu/GDY catalysts show high activity and selectivity toward H_2 in comparison with that in CORR, reflecting that the weaker binding of CO_2 than CO to Cu metal cannot effectively retard HER.^[23] For SAs, H_2 is a major product with a dominant FE at -1.0 V vs. RHE. As the size of Cu NCs increases, the activity and selectivity for CO are enhanced, while H_2 production is obviously suppressed. The influence of potentials on the product distribution is plotted using $\text{Cu}_{45.2}/\text{GDY}$ in Figure S17b. A FE_{CO} of 61.2% is achieved at -1.1 V vs. RHE while ethylene is in minute quantity even at larger potential. The exclusive C_1 products further indicate that the active sites were preserved under electrochemical reaction conditions and no reconstruction happened, in accordance with the observations in long-term electrolysis for CORR. Because all the restructuring behaviors of documented Cu catalysts, irrespective of the initial size of the active sites, will surely lead to the substantial conversion of CO_2 to C_{2+} and/or CH_4 .^[24] Such excellent stability for CO_2/CORR originates from the confinement environment from the hole enclosed by six triple bonds and the strong metal-support interaction from orbital overlaps^[13a] and electron transfer^[13b, 14] between Cu and C atoms. The structural property of 2D material, for example, a sandwich-like GDY-NCs-GDY structure, may play an essential role in stabilizing the NCs. So a suitable supporting material is indispensable to stabilize the geometric structure and electronic properties of active centers during electrolysis.^[25]

In order to consolidate the stability of catalysts further, the catalytic performance of $\text{Cu}_{45.2}/\text{GDY}$ after long-term (>22 h) CORR was evaluated toward CO_2RR (Figure S19). The switch to the CO_2 feed was operated immediately in situ after CORR. No obvious enhancement for C_2H_4 is observed compared to the as-prepared one, indicating that the catalyst remains intact even after long-term electrolysis. Our control experiments dispose of concerns that CO-induced surface restructuring into nanoparticles leads to the high C_{2+} selectivity toward CORR.^[26]

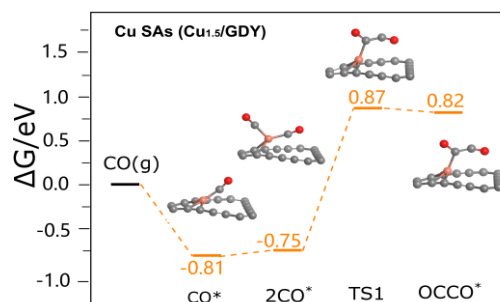


Figure 4. Free energy surfaces for CO coupling reactions on Cu SAs ($\text{Cu}_{1.5}/\text{GDY}$) and the correspondingly optimized structures of the intermediates.

We herein have attempted to rationalize the size effect on CO_2/CO electroreduction based on both our experimental observations and documented theoretical investigations. As the size of NCs decreases (to SAs), the great population of low coordinated single-sites result in stronger chemisorption of H^+ vs. CO_2 as compared to bulk Cu.^[3, 6, 27] This is the reason that the competing HER reaction is apparently enhanced as the size of Cu NCs decreased. But their weak binding of CO^* prevents subsequent deep reduction or coupling.^[17, 28] Therefore, only C_1 compounds and H_2 were obtained over Cu/GDY in CO_2RR . As for CORR, Back et al. concluded that single catalytic center of SAs facilitates the protonation of CO^* to CHO^* due to strong chemisorption of H^+ , multiple hydrogenation steps then take place on CHO^* , leading to the formation of CH_2O^* , CH_3O^* and ultimately CH_4 .^[29] The C–C coupling pathway between two C_1 species into one C_2 product is thermodynamically adverse due to the site competition. As is shown in Figure 4, the coupling of the two CO molecules to form OCCO^* is uphill by 1.57 eV with a barrier of 1.62 eV. Since the adsorption of the second CO is also endothermic, the effective barrier from CO^* to OCCO^* is 1.68 eV. The adsorption of the third CO is absolutely inhibited on Cu SAs. Accordingly, SAs shows the predominant C_1 selectivity during CORR. Large NCs are consisting of more undercoordinated Cu atoms and higher areal density at each cluster compared to SAs, which is beneficial for lowering free energy for C–C coupling,^[29c] allowing the reabsorption and dimerization of the CO or CO-derived intermediates spilling over to C_{2+} compounds.^[30] We demonstrate that cluster's size is of significant importance to CO_2/CORR . In view of little research on Cu NCs for CO_2/CORR , further studies might be necessary.

Conclusion

In summary, we synthesized a family of size-controlled Cu catalysts from single atoms to subnanometric clusters (0.5–1 nm) to nanoclusters (1–1.5 nm) on graphdiyne matrix via a creative acetylenic-bond-directed site-trapping approach. A clear correlation between the size of NCs in an atomic level and the catalytic performance could be inferred. For CO_2RR , larger nanocluster catalyst is more active and selective for CO over H_2 . For CORR, increasing the size of NCs will dramatically improve catalytic activity and selectivity for C_{2+} productions. The nanoclusters catalyst (1–1.5 nm) with the highest metal loading up to 45.2 wt %, represents the first GDY-supported nanoclusters to access high C_{2+} activity and selectivity toward

CORR, comparable to the performance of the current state-of-the-art CO reduction catalysts. The exceptional performances of Cu NCs are attributed to both the larger population of low-coordinated atoms and the lower free energy for C-C coupling. The comparison between CO and CO₂ reduction clearly demonstrates the potential advantages of CO electrolysis to produce valuable C₂₊ chemicals. The outstanding stability can be explained by the strong Cu-C coordination and confinement effects from the GDY support. Last but not least, the acetylenic-bond-directed site-trapping strategy paves the way to synthesize other transition metal-based nanoclusters, representing a step forward to large scale application of metal NCs for renewable energy storage.

Experimental Section

Materials: THF was freshly distilled from sodium benzophenone ketyl under Ar and stored over sodium. Cuprous iodide (CuI) and Tetrabutylammonium fluoride (TBAF, 1.0 M in THF) were purchased from Sigma Aldrich. The water used was purified with a Millipore system (typically 18.2 MΩ cm resistivity). Gas diffusion layers (GDL) were purchased from Fuel Cell Store with Sigracet 29 BC model. IrO₂-coating titanium sheet as the counter electrode was purchased from Baoji Zhiming Special Metal Co., LTD. Hexakis(trimethylsilyl)ethynylbenzene and GDY were synthesized according to the reported methods.^[11]

Synthesis of catalysts Cu/GDY: The catalysts were synthesized under a dry and oxygen-free argon atmosphere by using the Schlenk technique. To a solution of hexakis(trimethylsilyl)ethynylbenzene (43.6 mg, 0.066 mmol) in dry THF (15 ml) was added dropwise 0.4 mL of TBAF (1.0 M in THF, 0.4 mmol) and stirred at -78 °C for 30 min. The solution was transferred to a suspension of cuprous iodide (75 mg for Cu_{45.2}/GDY; 3.3 mg for Cu_{6.0}/GDY; 0.8 mg for Cu_{1.5}/GDY) in THF. The mixture was allowed to warm to room temperature with a violent stirring and then heated at 60 °C for 7 days. The precipitate was separated by centrifugation, washed by acetone, ethanol and water, and dried in vacuum overnight to yield the corresponding catalysts as brown to black powders.

Acknowledgements

This work is supported by the National Natural Science Foundation of China (21771098, 21903016), the Science and Technology Innovation Commission of Shenzhen Municipality (JCYJ20170817111548026), Shenzhen Clean Energy Research Institute (No. CERI-KY-2019-003) and the Shenzhen Nobel Prize Scientists Laboratory Project (C17783101) and Guangdong Provincial Key Laboratory of Energy Materials for Electric Power (2018B030322001).

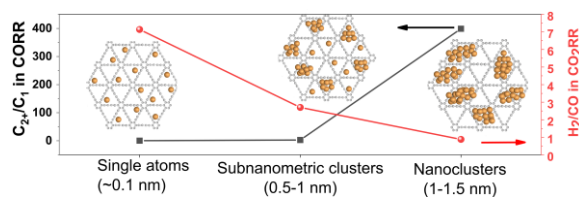
Keywords: size effect • CO₂/CO electroreduction • Cu nanoclusters • single atoms • graphdiyne

- [1] M. B. Ross, P. De Luna, Y. Li, C.-T. Dinh, D. Kim, P. Yang, E. H. Sargent, *Nat. Catal.* **2019**, *2*, 648–658.
 [2] a) T.-T. Zhuang, Y. Pang, Z.-Q. Liang, Z. Wang, Y. Li, C.-S. Tan, J. Li, C. T. Dinh, P. De Luna, P.-L. Hsieh, T. Burdyny, H.-H. Li, M. Liu, Y. Wang, F. Li, A. Proppe, A. Johnston, D.-H. Nam, Z.-Y. Wu, Y.-R. Zheng,

- A. H. Ip, H. Tan, L.-J. Chen, S.-H. Yu, S. O. Kelley, D. Sinton, E. H. Sargent, *Nat. Catal.* **2018**, *1*, 946–951; b) Y. Pang, J. Li, Z. Wang, C.-S. Tan, P.-L. Hsieh, T.-T. Zhuang, Z.-Q. Liang, C. Zou, X. Wang, P. De Luna, J. P. Edwards, Y. Xu, F. Li, C.-T. Dinh, M. Zhong, Y. Lou, D. Wu, L.-J. Chen, E. H. Sargent, D. Sinton, *Nat. Catal.* **2019**, *2*, 251–258; c) W. Luc, X. Fu, J. Shi, J.-J. Lv, M. Jouny, B. H. Ko, Y. Xu, Q. Tu, X. Hu, J. Wu, Q. Yue, Y. Liu, F. Jiao, Y. Kang, *Nat. Catal.* **2019**, *2*, 423–430.
 [3] R. Reske, H. Mistry, F. Behafarid, B. Roldan Cuenya, P. Strasser, *J. Am. Chem. Soc.* **2014**, *136*, 6978–6986.
 [4] I. Merino-Garcia, J. Albo, A. Irabien, *Nanotechnology* **2018**, *29*, 014001.
 [5] S. Nitopi, E. Bertheussen, S. B. Scott, X. Liu, A. K. Engstfeld, S. Horch, B. Seger, I. E. L. Stephens, K. Chan, C. Hahn, J. K. Nørskov, T. F. Jaramillo, I. Chorkendorff, *Chem. Rev.* **2019**, *119*, 7610–7672.
 [6] D. Gao, R. M. Arán-Ais, H. S. Jeon, B. Roldan Cuenya, *Nat. Catal.* **2019**, *2*, 198–210.
 [7] X. Liu, D. Astruc, *Coord. Chem. Rev.* **2018**, *359*, 112–126.
 [8] a) C. Liu, H. He, P. Zapol, L. A. Curtiss, *Phys. Chem. Chem. Phys.* **2014**, *16*, 26584–26599; b) Y. F. Bu, M. Zhao, G. X. Zhang, X. Zhang, W. Gao, Q. Jiang, *ChemElectroChem* **2019**, *6*, 1831–1837; c) X. Bai, Q. Li, L. Shi, X. Niu, C. Ling, J. Wang, *Small* **2020**, *16*, e1901981.
 [9] a) Q. Tang, Y. Lee, D. Y. Li, W. Choi, C. W. Liu, D. Lee, D. E. Jiang, *J. Am. Chem. Soc.* **2017**, *139*, 9728–9736; b) Q. Hu, Z. Han, X. Wang, G. Li, Z. Wang, X. Huang, H. Yang, X. Ren, Q. Zhang, J. Liu, C. He, *Angew. Chem. Int. Ed.* 10.1002/anie.202009277.
 [10] H. Qi, P. Yu, Y. Wang, G. Han, H. Liu, Y. Yi, Y. Li, L. Mao, *J. Am. Chem. Soc.* **2015**, *137*, 5260–5263.
 [11] G. Li, Y. Li, H. Liu, Y. Guo, Y. Li, D. Zhu, *Chem. Commun.* **2010**, *46*, 3256–3258.
 [12] a) R. Sakamoto, N. Fukui, H. Maeda, R. Matsuoka, R. Toyoda, H. Nishihara, *Adv. Mater.* **2019**, *31*, e1804211; b) C. Huang, Y. Li, N. Wang, Y. Xue, Z. Zuo, H. Liu, Y. Li, *Chem. Rev.* **2018**, *118*, 7744–7803.
 [13] a) Y. Xue, B. Huang, Y. Yi, Y. Guo, Z. Zuo, Y. Li, Z. Jia, H. Liu, Y. Li, *Nat. Commun.* **2018**, *9*, 1460; b) H. Yu, Y. Xue, B. Huang, L. Hui, C. Zhang, Y. Fang, Y. Liu, Y. Zhao, Y. Li, H. Liu, Y. Li, *iScience* **2019**, *11*, 31–41; c) Y. Gao, Z. Cai, X. Wu, Z. Lv, P. Wu, C. Cai, *ACS Catal.* **2018**, *8*, 10364–10374; d) X. P. Yin, H. J. Wang, S. F. Tang, X. L. Lu, M. Shu, R. Si, T. B. Lu, *Angew. Chem.* **2018**, *130*, 9526–9530; *Angew. Chem. Int. Ed.* **2018**, *57*, 9382–9386.
 [14] Y. Xue, J. Li, Z. Xue, Y. Li, H. Liu, D. Li, W. Yang, Y. Li, *ACS Appl. Mater. Interfaces* **2016**, *8*, 31083–31091.
 [15] a) Y. Lu, W. Wei, W. Chen, *Chin. Sci. Bull.* **2012**, *57*, 41–47; b) C. Lu, R. Fang, X. Chen, *Adv. Mater.* **2020**, *32*, e1906548.
 [16] D. Ma, Z. Zeng, L. Liu, X. Huang, Y. Jia, *J. Phys. Chem. C* **2019**, *123*, 19066–19076.
 [17] W. Ju, A. Bagger, G. P. Hao, A. S. Varela, I. Sinev, V. Bon, B. Roldan Cuenya, S. Kaskel, J. Rossmel, P. Strasser, *Nat. Commun.* **2017**, *8*, 944.
 [18] J. Li, L. Zhong, L. Tong, Y. Yu, Q. Liu, S. Zhang, C. Yin, L. Qiao, S. Li, R. Si, J. Zhang, *Adv. Funct. Mater.* **2019**, *29*, 1905423.
 [19] a) H. Yang, Y. Wu, G. Li, Q. Lin, Q. Hu, Q. Zhang, J. Liu, C. He, *J. Am. Chem. Soc.* **2019**, *141*, 12717–12723; b) F. Huang, Y. Deng, Y. Chen, X. Cai, M. Peng, Z. Jia, J. Xie, D. Xiao, X. Wen, N. Wang, Z. Jiang, H. Liu, D. Ma, *Nat. Commun.* **2019**, *10*, 4431; c) Y. Qu, Z. Li, W. Chen, Y. Lin, T. Yuan, Z. Yang, C. Zhao, J. Wang, C. Zhao, X. Wang, F. Zhou, Z. Zhuang, Y. Wu, Y. Li, *Nat. Catal.* **2018**, *1*, 781–786.
 [20] M. Jouny, G. S. Hutchings, F. Jiao, *Nat. Catal.* **2019**, *2*, 1062–1070.
 [21] M. Jouny, W. Luc, F. Jiao, *Nat. Catal.* **2018**, *1*, 748–755.
 [22] L. Han, W. Zhou, C. Xiang, *ACS Energy Lett.* **2018**, *3*, 855–860.
 [23] T. Cheng, H. Xiao, W. A. Goddard, 3rd, *Proc. Natl. Acad. Sci. U S A* **2017**, *114*, 1795–1800.
 [24] a) D. Kim, C. S. Kley, Y. Li, P. Yang, *Proc. Natl. Acad. Sci. U S A* **2017**, *114*, 10560–10565; b) Y.-G. Kim, A. Javier, J. H. Baricuatro, M. P. Soriaga, *Electrocatalysis* **2016**, *7*, 391–399; c) Y.-G. Kim, A. Javier, J. H. Baricuatro, D. Torelli, K. D. Cummins, C. F. Tsang, J. C. Hemminger, M. P. Soriaga, *J. Electroanal. Chem.* **2016**, *780*, 290–295; d) Y. Li, F. Cui, M. B. Ross, D. Kim, Y. Sun, P. Yang, *Nano Lett.* **2017**, *17*, 1312–1317; e) P. Grosse, D. Gao, F. Scholten, I. Sinev, H. Mistry, B. Roldan Cuenya, *Angew. Chem.* **2018**, *130*, 6300–6305; *Angew. Chem. Int. Ed.* **2018**, *57*, 6192–6197; f) D. Karapinar, N. T. Huan, N. Ranjbar Sahraie,

- J. Li, D. Wakerley, N. Touati, S. Zanna, D. Taverna, L. H. Galvão Tizei, A. Zitolo, F. Jaouen, V. Mougel, M. Fontecave, *Angew. Chem.* **2019**, *131*, 15242–15247; *Angew. Chem. Int. Ed.* **2019**, *58*, 15098–15103; g) H. Jung, S. Y. Lee, C. W. Lee, M. K. Cho, D. H. Won, C. Kim, H. S. Oh, B. K. Min, Y. J. Hwang, *J. Am. Chem. Soc.* **2019**, *141*, 4624–4633; h) M. Balamurugan, H. Y. Jeong, V. S. K. Choutipalli, J. S. Hong, H. Seo, N. Saravanan, J. H. Jang, K. G. Lee, Y. H. Lee, S. W. Im, V. Subramanian, S. H. Kim, K. T. Nam, *Small* **2020**, *16*, e2000955; i) Z. Weng, Y. Wu, M. Wang, J. Jiang, K. Yang, S. Huo, X. F. Wang, Q. Ma, G. W. Brudvig, V. S. Batista, Y. Liang, Z. Feng, H. Wang, *Nat. Commun.* **2018**, *9*, 415; j) H. Xu, D. Rebolgar, H. He, L. Chong, Y. Liu, C. Liu, C.-J. Sun, T. Li, J. V. Muntean, R. E. Winans, D.-J. Liu, T. Xu, *Nat. Energy* 10.1038/s41560-020-0666-x.
- [25] L. Tang, X. Meng, D. Deng, X. Bao, *Adv. Mater.* **2019**, 1901996.
- [26] a) B. Eren, D. Zherebetsky, L. L. Patera, C. H. Wu, H. Bluhm, C. Africh, L. Wang, G. A. Somorjai, M. Salmeron, *Science* **2016**, *351*, 475–478; b) C. M. Gunathunge, X. Li, J. Li, R. P. Hicks, V. J. O'valle, M. M. Waegle, *J. Phys. Chem. C* **2017**, *121*, 12337–12344.
- [27] A. D. Handoko, F. Wei, Jenndy, B. S. Yeo, Z. W. Seh, *Nat. Catal.* **2018**, *1*, 922–934.
- [28] X. Liu, P. Schlexer, J. Xiao, Y. Ji, L. Wang, R. B. Sandberg, M. Tang, K. S. Brown, H. Peng, S. Ringe, C. Hahn, T. F. Jaramillo, J. K. Nørskov, K. Chan, *Nat. Commun.* **2019**, *10*, 32.
- [29] a) A. Vasileff, C. Xu, Y. Jiao, Y. Zheng, S.-Z. Qiao, *Chem* **2018**, *4*, 1809–1831; b) S. Back, J. Lim, N. Y. Kim, Y. H. Kim, Y. Jung, *Chem Sci* **2017**, *8*, 1090–1096; c) A. Guan, Z. Chen, Y. Quan, C. Peng, Z. Wang, T.-K. Sham, C. Yang, Y. Ji, L. Qian, X. Xu, G. Zheng, *ACS Energy Lett.* **2020**, *5*, 1044–1053.
- [30] a) H. Mistry, F. Behafarid, R. Reske, A. S. Varela, P. Strasser, B. Roldan Cuenya, *ACS Catal.* **2016**, *6*, 1075–1080; b) X. Wang, A. S. Varela, A. Bergmann, S. Kuhl, P. Strasser, *ChemSusChem* **2017**, *10*, 4642–4649.

Entry for the Table of Contents



The size-controlled Cu catalysts from single atoms to subnanometric clusters (0.5–1 nm) to nanoclusters (1–1.5 nm) on graphdiyne matrix are readily prepared via a creative acetylenic-bond-directed site-trapping approach. A clear size dependence of activity and selectivity toward CO/CO₂RR over these atomic-level catalysts has been demonstrated for the first time.